Letter

Complex magnetic and spatial symmetry breaking from correlations in kagome flat bands

Yu-Ping Lin,[1] Chunxiao Liu,[1] and Joel E. Moore[1,2]
[1]*Department of Physics, University of California, Berkeley, California 94720, USA*
[2]*Materials Sciences Division, Lawrence Berkeley National Laboratory, Berkeley, California 94720, USA*

(Received 17 August 2023; revised 14 May 2024; accepted 9 July 2024; published 29 July 2024)

We present the mean-field phase diagram of electrons in a kagome flat band with repulsive interactions. In addition to flat-band ferromagnetism, the Hartree-Fock analysis yields cascades of unconventional magnetic orders driven by on-site repulsion as filling changes. These include a series of antiferromagnetic (AFM) spin-charge stripe orders, as well as an evolution from 120° AFM to intriguing noncoplanar spin orders with tetrahedral structures. We also map out the phase diagram under extended repulsion at half and empty fillings of the flat band. To examine the possibilities beyond the mean-field level, we conduct a projective symmetry group analysis and identify the feasible $\mathbb{Z}_2$ spin liquids and the magnetic orders derivable from them. The theoretical phase diagrams are compared with recent experiments on FeSn and FeGe, enabling a determination of the most likely magnetic instabilities in these and similar flat-band kagome materials.

DOI: 10.1103/PhysRevB.110.L041121

Introduction. The study of flat bands has become a major focus of condensed-matter research in the past decade. Among various flat-band systems, there is a family in which the flat bands are inherent to geometric frustration of the lattices [1–9]. Under the destructive interference of hoppings, compact localized states (CLSs) appear as dispersionless eigenstates and form the flat bands, in combination with noncontractible loop states. The search among frustrated materials has identified many candidates. In particular, recent experiments have observed (approximately) flat bands in the quasi-two-dimensional (2D) kagome metals FeSn [10] and CoSn [11] and their relevance to FeGe [12–14].

The kagome lattice is known as a fruitful basis for correlated phases. In particular, the massive density of states carried by the flat band can enhance correlation effects, giving rise to a rich phase diagram. The famous Stoner criterion for ferromagnetism (FM) [15] can be easily satisfied, supposedly accounting for the intralayer FM below 300–400 K in FeSn [10,16] and FeGe [12–14]. Interestingly, FeGe further shows a charge density wave (CDW) below 100 K [12–14], similar to the nonmagnetic kagome metals AV_3Sb_5 with $A =$ K, Rb, and Cs [17,18]. FM is proposed to be the ground state under on-site repulsion in the kagome flat band, especially at and above half filling [1,19–21]. Meanwhile, the large number of kagome materials suggests an opportunity for many other correlated phases to be explored. Various unconventional correlated phases, such as quantum anomalous Hall FM (QAHFM) and combinations of spin and charge orders, have been proposed at spinful half filling [22], spinless [23–27] or spinful [25,28,29] empty filling, and fractional filling under topology [30,31].

Given the rich range of correlated phases in both experiment and theory, it is natural to seek the interaction-driven phase diagram in the kagome flat band. In this Letter, we conduct various theoretical analyses to achieve this goal. Our central result is a mean-field phase diagram obtained through Hartree-Fock analysis. This phase diagram, as shown in Fig. 1, is controlled by on-site repulsion and electron filling. We highlight that our Hartree-Fock analysis, compared with previous works [20,25,28], does not impose any symmetry constraints or *Ansätze*. This fully unrestricted approach allows us to uncover many unconventional ordered states existing in the phase diagram (Fig. 1). Interestingly, we find doping cascades of spin-charge (S-C) stripe and 120° antiferromagnetic (AFM) to noncoplanar spin (NCPS) orders, which fill the weak-to-moderate-coupling regime below half filling [20]. Adding extended repulsions further expands the phase diagrams at half [22] and empty fillings [25,28]. Going beyond the mean-field level, we conduct a projective symmetry group (PSG) analysis, thereby identifying a $\mathbb{Z}_2$ spin liquid whose derived magnetic orders match the Hartree-Fock results. Finally, by comparing our theory with existing experiments on FeSn and FeGe, we guide the search for unconventional ordering in future studies of flat-band kagome metals.

Kagome lattice and flat band. We study the repulsive fermionic Hubbard model [32,33] on the kagome lattice [Fig. 2(a)]

$$H = -\sum_{ii'\tau\tau'}\sum_{\sigma} t_{ii'\tau\tau'} c^{\dagger}_{i\tau\sigma} c_{i'\tau'\sigma} + \frac{1}{2}\sum_{ii'\tau\tau'}\sum_{\sigma\sigma'} U_{ii'\tau\tau'} c^{\dagger}_{i\tau\sigma} c^{\dagger}_{i'\tau'\sigma'} c_{i'\tau'\sigma'} c_{i\tau\sigma}, \quad (1)$$

where $c^{(\dagger)}_{i\tau\sigma}$ annihilates (creates) a fermion at the Bravais-lattice site i and sublattice $\tau = 0, 1, 2$ with spin $\sigma = \uparrow\downarrow$. The tight-binding hoppings $t_{ii'\tau\tau'}$ and density-density repulsions $U_{ii'\tau\tau'}$ are defined according to their ranges of action as on-site t_0 and U_0, nearest-neighbor t_1 and U_1, second-neighbor t_2 and U_2, etc.

The tight-binding Hamiltonian hosts three bands in the Brillouin zone [Figs. 2(b) and 2(c)]. The topmost band is completely flat under nearest-neighbor hopping $t_1 > 0$ [1,2]. Focusing on this flat band, we define the flat-band (FB) filling

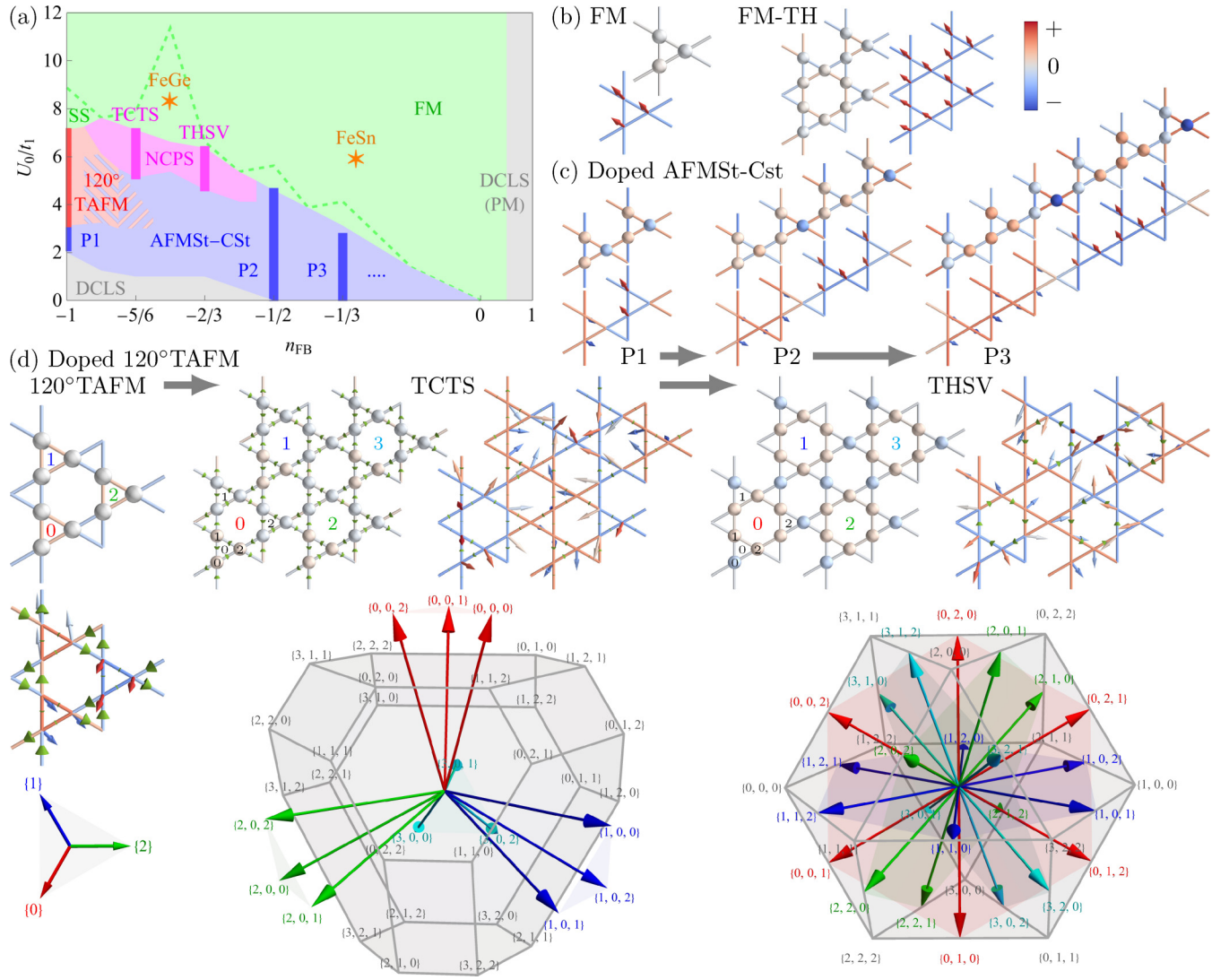

FIG. 1. Mean-field phase diagram in a kagome flat band. (a) The phase diagram of the pure Hubbard model. The colored bars indicate commensurate-filling orders, and the hatches indicate phase separation. (b)–(d) S-C patterns of the ground states. For the charge patterns, the warm (cool) colors indicate higher (lower) densities on the sites and bonds from their averages (see the color bar). The green bond arrowheads indicate the bond currents. For the spin patterns, the site arrows represent in-plane components, while the colors indicate out-of-plane components on both sites and bonds. The bond arrowheads again indicate the bond currents. In the noncollinear spin orders (d), the spin structures are further presented. The arrow colors match the labels of chosen cells. The labels for 120°TAFM apply to the 1-triangle cells. For the TCTS and THSV orders, the labels {3-triangle cell, 1-triangle cell, site} are defined. The colored arrows and gray-polyhedron corners represent the spins on high- and low-density sites, respectively.

$n_{FB} \in [-1, 1]$. Half filling is $n_{FB} = 0$, and $n_{FB} = \pm 1$ correspond to full and empty fillings, respectively.

Mean-field phase diagram. We employ the Hartree-Fock analysis to obtain the repulsion-driven ground states at the mean-field level. Our spatially unrestricted formalism [34] is effective for unbiased search of symmetry-breaking ground states with enlarged unit cells. We first focus on the pure Hubbard model with nearest-neighbor hopping $t_1 = 1$ and on-site repulsion $U_0 > 0$. Sweeping across all flat-band fillings, we map out the n_{FB}-U_0 phase diagram [Fig. 1(a)]. One immediate observation is the wide FM phase [Fig. 1(b)] at strong coupling [20], which extends to the weak-coupling limit $U_0 = 0$ at and above half filling $n_{FB} \geqslant 0$. Meanwhile, the other competing orders arise at weak-to-moderate coupling below half filling $n_{FB} < 0$.

Ferromagnetism. When FM develops, the bands split into majority- and minority-spin branches. The density imbalance $\delta n_S = n_{major} - n_{minor}$ determines the energy of this Stoner splitting

$$\Delta E_S = U_0 \delta n_S. \tag{2}$$

To saturate the maximal magnetization $m = \delta n_S/2$, the Stoner splitting should fully fill the majority-spin bands by pushing them below the minority-spin Fermi level. For half filling $n_{FB} = 0$, the saturated minority-spin Fermi level lies at the quadratic band-crossing point (QBCP) Γ [Fig. 2(d)]. The saturation occurs under arbitrarily small repulsion, indicating a strong weak-coupling instability towards FM. This scenario also applies above half filling $n_{FB} > 0$. On the other hand, the saturation splitting increases below half filling $n_{FB} < 0$,

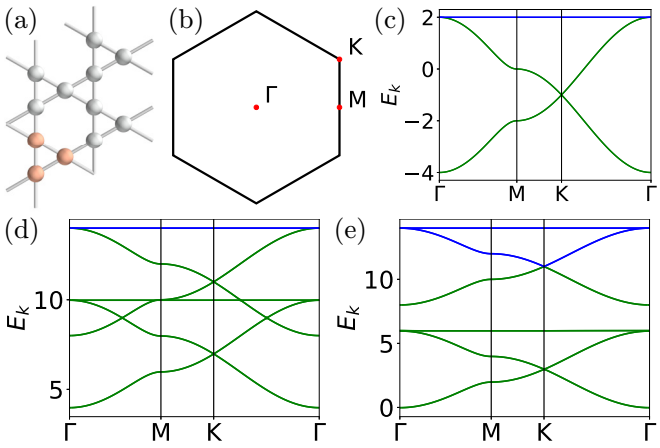

FIG. 2. Kagome lattice. (a) The lattice with a unit cell marked (orange). The triangular-Bravais-lattice vectors are $\mathbf{a}_1 = (0, 2)$ and $\mathbf{a}_2 = (\sqrt{3}, 1)$ with intersite distance 1. (b) The Brillouin zone and high-symmetry points. (c) The band structure with filled (green) and empty (blue) band segments. (d),(e) The FM band structures with $U_0/t = 12$ at $n_{\mathrm{FB}} = 0$ and -1.

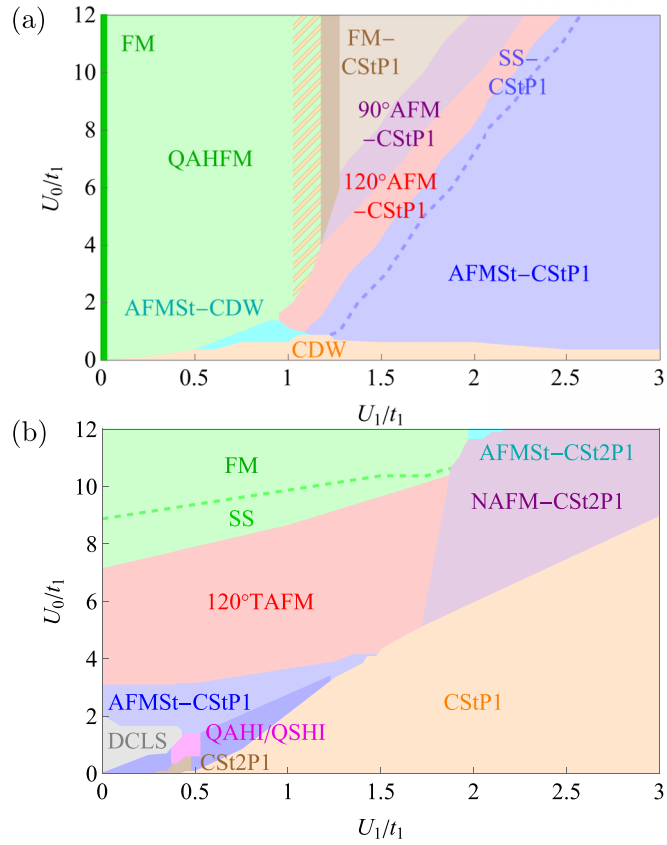

FIG. 3. Extended-repulsion phase diagrams at (a) half filling $n_{\mathrm{FB}} = 0$ and (b) empty filling $n_{\mathrm{FB}} = -1$.

with the maximum at empty filling $n_{\mathrm{FB}} = -1$ [Fig. 2(e)]. The FM is destabilized gradually, giving way to other competing orders at weak-to-moderate coupling. Note that the FM in the phase diagram [Fig. 1(a)] is always saturated and is a half (semi)metal.

Competing orders. Next we explore the plethora of phases below half filling, $n_{\mathrm{FB}} < 0$. We begin with the moderate-coupling regime at empty filling, $n_{\mathrm{FB}} = -1$. An **M**-point S-C stripe order arises at $U_0 = 2$. Here AFM stripes develop on charge nematic high-density stripes and form an AFM-stripe-charge-stripe-period-1 (AFMSt-CStP1) pattern [Fig. 1(c)]. For $U_0 \geqslant 3$, the ground state is taken over by a **K**-point order. This order shows a $\sqrt{3} \times \sqrt{3}$ 120° triangle AFM (120° TAFM) [Fig. 1(d)], where coplanar 120° order [35] forms among three nearest-neighbor triangles.

Cascade of S-C stripe orders. Moving away from empty filling, $n_{\mathrm{FB}} = -1$, many orders appear. In the S-C-stripe regime, the AFMSt-CStP1 order deforms into the FM as n_{FB} goes from -1 to 0. Intuitively, the FM is an AFMSt-CSt order with infinite period (P∞). There is an elegant cascade of Pn orders at the reciprocal integer fillings $n_{\mathrm{FB}} = -1/n$ [Fig. 1(c)], where one out of n low-density stripes is unfilled at $n_{\mathrm{FB}} = -1/n$. Note that the cascade is also visible away from the reciprocal integer fillings $n_{\mathrm{FB}} = -1/n$ [34], despite some intertwinement with the 120° TAFM.

Cascade of noncoplanar spin orders. More intriguing magnetic orders appear when the 120° TAFM is doped. Remarkably, the energetically favorable path breaks coplanarity and travels through noncoplanar spin orders. At commensurate fillings $n_{\mathrm{FB}} = -5/6$ and $-2/3$, which are 1/3 and 2/3 between $n_{\mathrm{FB}} = -1$ and $-1/2$, we observe enriched tetrahedral spin orders [Fig. 1(d)]. The S-C unit cell is $2\sqrt{3} \times 2\sqrt{3}$ at both fillings. The charge unit cell is $\sqrt{3} \times \sqrt{3}$, containing both high- and low-density sites. The tetrahedral spin orders further enlarge the period by 2×2. At $n_{\mathrm{FB}} = -5/6$, each high-density triangle hosts C_3-symmetric canted spins about a principal order. The principal orders are tetrahedral, making the ground state a tetrahedral canted triangle-spin (TCTS) order. Note that the low-density sites also host TCTS structures, which couple to the high-density TCTS order and induce the canting. At $n_{\mathrm{FB}} = -2/3$, we observe a coplanar 2π spin winding on each high-density hexagon, which we term the hexagon spin vortex (HSV). Amazingly, the HSVs are again tetrahedral, and the ground state is a tetrahedral HSV (THSV) order. This order is actually a canted tripling of the cuboc order in the classical J_1-J_2 model [36–38]. The low-density kagome superlattice hosts the 12-site cuboc order. Meanwhile, the high-density sites show a 24-site canted doubling, where each spin is the middle of its two low-density neighbors.

Due to nontrivial spin configurations, noncollinear spin orders may act as sources of time-reversal-symmetry-breaking fluxes, thereby inducing nontrivial band topology [39–42]. To examine the possibility of noncollinear-spin Chern insulators, we conduct a thorough band-structure computation [34]. Remarkably, we find nonzero quantized Chern number $C = \pm 1$ for the TCTS order, consistent with nonzero scalar spin chirality from noncoplanar spin textures [39–42].

Completion of phase diagram. The phase diagram [Fig. 1(a)] exhibits a few more features apart from the uniform orders, including phase separation [20,43,44], coplanar spiral spin (SS) orders [20,44], and dilute CLS (DCLS). Furthermore, we go beyond the pure Hubbard model by adding extended repulsions $U_1 = 2U_2 > 0$ (Fig. 3). While on-site repulsion favors magnetic orders, extended repulsion enhances

TABLE I. Summary of magnetic orders derived from the PSG classes (0,1) and (1,0). Ordering structure in the enlarged magnetic unit cell: †: nonuniform, umbrella order. ‡: Coplanar 120°. The cases 1, 2, and 3–5 of class (1,0) correspond to the FM, 120° TAFM, and SS orders in the Hartree-Fock analysis, respectively.

Class	No.	Spinon k_c	Mag. unit cell	Sublattice structure
(0,1)	1	Γ	Not enlarged	Collinear
	2	Γ	Not enlarged	Collinear
	3	$\pm K$	$\sqrt{3}\times\sqrt{3}^{\dagger}$	Collinear
	4	$\pm K$	$\sqrt{3}\times\sqrt{3}^{\dagger}$	Coplanar 120°
	5	$M_{1,2,3}$	$2\times 2^{\dagger}$	τ-M_τ-locked stripe
(1,0)	1	Γ	Not enlarged	Collinear
	2	$\pm K$	$\sqrt{3}\times\sqrt{3}^{\ddagger}$	Collinear
	3–5	$\Gamma \leftrightarrow \pm K$ $\leftrightarrow M_{1,2,3}$	Incommensurate	

charge orders and alters the ground states. See Supplemental Material [34] for the detailed discussions.

Possible spin liquids. The rich structure in the phase diagrams reveals an intricate relation among the competing magnetic orders. An interesting scenario may happen when they arise as symmetry-breaking instabilities of a *parent* quantum spin liquid [45]. Here, from a symmetry perspective, we explore this possibility by selecting the most likely $\mathbb{Z}_2$ kagome spin liquids [46–49] and analyzing the various magnetic orders derived from them [34,50].

Our starting point is the two Z_2-spin-liquid Hamiltonians obtained from the PSG classification [51] for bosonic spinons. This conveniently allows us to consider the leading instability upon condensing the spinons. The resulting orders are given in Table I. Starting from the (1,0) class of $\mathbb{Z}_2$ parent spin liquid, we reproduce the FM, 120° TAFM, and SS orders in Hartree-Fock analysis [52]. Crucially, the SS orders are much weaker, suggesting the possible discovery of $\mathbb{Z}_2$ parent spin liquid in its mean-field phase region [Fig. 1(a)]. On the other hand, we find an interesting sublattice-momentum-locked magnetic order from the (0,1) class. This magnetic order may share similar structure to the tetrahedral chiral spin density wave [41].

Experimental realization. We examine the flat-band kagome metals FeSn [10] and FeGe [12–14] in light of our phase diagrams. Motivated by the Fe-$d_{xz/yz}$-orbital band structures of FeSn [16] and FeGe [assuming the Van Hove singularity (VHS) at the Fermi level as was experimentally observed] [14] in first-principles computations, we consider the single-orbital pure Hubbard model on the kagome lattice. The flat-band filling n_{FB} and the on-site repulsion U_0 are estimated from the minority-spin filling and Stoner splitting energy (2), respectively. This estimation locates FeSn and FeGe in our phase diagram, as shown in Fig. 1(a). FeSn falls in the FM phase, consistent with the experiments. Although FeGe sits in the SS-order phase, the interlayer and multiorbital effects may stabilize the FM. We further include the nearest-neighbor repulsion $U_1/t_1 \approx 1.07$ for FeGe by fitting the CDW splitting [14]. This induces the secondary tri-hexagonal bond order (FM-TH) [Fig. 1(b)], consistent with the experimental 2×2 CDW [12–14] and the theoretical CDW at VHS [53–57].

It is worth noting the possible implications of the results in our work. The majority of existing compounds (such as FeSn and FeGe) are located in the large-U_0 FM phase. Meanwhile, our analysis finds intriguing magnetic orders at smaller repulsion U_0. We thus propose the reduction of electronic repulsion as a feasible route toward unconventional magnetism in a kagome flat band. In addition to the binary compounds AB, another feasible family is the ternary series AB_3C_5. These materials host possibly weaker correlations than FeSn and FeGe, and the Fermi level can be tuned flexibly by element substitutions [58]. On the other hand, with the ultracold-atom simulation of a kagome lattice [59], the flat-band correlated phases can be induced by adding the Hubbard interaction [60].

Discussion. Our analysis includes a detailed study of kagome flat bands at the mean-field level, but there remains a considerable scope for further investigation. First, the Hartree-Fock analysis can overestimate the symmetry-breaking orders and miss essential intertwinement between different orders. While the former may be less serious in the flat band, the latter may be enhanced due to strong correlations. Second, there are important correlated phases that are not captured. These include superconductivity, which does not appear at the mean-field level under electronic repulsion. It will be interesting to search for superconductivity by doping the unconventional magnetic orders [61–66] in our phase diagram. Meanwhile, spin-triplet superconductivity may occur in the FM half metal [67–69]. On the other hand, the ground states away from the fermion-bilinear condensates, such as spin liquids [70] and fractional Chern insulators [71], are also invisible. While we suggest candidate $\mathbb{Z}_2$ spin liquids with a PSG analysis, a future confirmation with strong-correlation numerical methods will be informative.

Note added. After the original version of this work, the synthesis of $CsCr_3Sb_5$ in the AB_3C_5 kagome family was reported [72]. A non-FM S-C-density-wave order develops close to the flat band, consistent with expectations from our Hartree-Fock analysis.

Acknowledgments. The authors thank Shubhayu Chatterjee, Yi-Ping Huang, Haining Pan, and Linda Ye for fruitful discussions. This work was primarily supported by the Air Force Office of Scientific Research under Grant No. FA9550-22-1-0270. Y.P.L. and C.L. acknowledge fellowship support from the Gordon and Betty Moore Foundation through the Emergent Phenomena in Quantum Systems (EPiQS) program. J.E.M. acknowledges a Simons Investigatorship. Parts of the numerical computations were performed on the Lawrencium cluster at Lawrence Berkeley National Laboratory.

[1] A. Mielke, Exact ground states for the Hubbard model on the kagome lattice, J. Phys. A **25**, 4335 (1992).

[2] D. L. Bergman, C. Wu, and L. Balents, Band touching from real-space topology in frustrated hopping models, Phys. Rev. B **78**, 125104 (2008).

[3] D. Leykam, A. Andreanov, and S. Flach, Artificial flat band systems: from lattice models to experiments, Adv. Phys. X **3**, 1473052 (2018).

[4] W. Maimaiti, A. Andreanov, and S. Flach, Flat-band generator in two dimensions, Phys. Rev. B **103**, 165116 (2021).

[5] D. Călugăru, A. Chew, L. Elcoro, Y. Xu, N. Regnault, Z.-D. Song, and B. A. Bernevig, General construction and topological classification of crystalline flat bands, Nat. Phys. **18**, 185 (2022).

[6] N. Regnault, Y. Xu, M.-R. Li, D.-S. Ma, M. Jovanovic, A. Yazdani, S. S. P. Parkin, C. Felser, L. M. Schoop, N. P. Ong, R. J. Cava, L. Elcoro, Z.-D. Song, and B. A. Bernevig, Catalogue of flat-band stoichiometric materials, Nature (London) **603**, 824 (2022).

[7] A. Graf and F. Piéchon, Designing flat-band tight-binding models with tunable multifold band touching points, Phys. Rev. B **104**, 195128 (2021).

[8] Y. Hwang, J.-W. Rhim, and B.-J. Yang, General construction of flat bands with and without band crossings based on wave function singularity, Phys. Rev. B **104**, 085144 (2021).

[9] P. M. Neves, J. P. Wakefield, S. Fang, H. Nguyen, L. Ye, and J. G. Checkelsky, Crystal net catalog of model flat band materials, npj Comput. Mater. **10**, 39 (2024).

[10] M. Kang, L. Ye, S. Fang, J.-S. You, A. Levitan, M. Han, J. I. Facio, C. Jozwiak, A. Bostwick, E. Rotenberg, M. K. Chan, R. D. McDonald, D. Graf, K. Kaznatcheev, E. Vescovo, D. C. Bell, E. Kaxiras, J. van den Brink, M. Richter, M. Prasad Ghimire *et al.*, Dirac fermions and flat bands in the ideal kagome metal FeSn, Nat. Mater. **19**, 163 (2020).

[11] M. Kang, S. Fang, L. Ye, H. C. Po, J. Denlinger, C. Jozwiak, A. Bostwick, E. Rotenberg, E. Kaxiras, J. G. Checkelsky, and R. Comin, Topological flat bands in frustrated kagome lattice CoSn, Nat. Commun. **11**, 4004 (2020).

[12] X. Teng, L. Chen, F. Ye, E. Rosenberg, Z. Liu, J.-X. Yin, Y.-X. Jiang, J. S. Oh, M. Z. Hasan, K. J. Neubauer, B. Gao, Y. Xie, M. Hashimoto, D. Lu, C. Jozwiak, A. Bostwick, E. Rotenberg, R. J. Birgeneau, J.-H. Chu, M. Yi *et al.*, Discovery of charge density wave in a kagome lattice antiferromagnet, Nature (London) **609**, 490 (2022).

[13] J.-X. Yin, Y.-X. Jiang, X. Teng, M. S. Hossain, S. Mardanya, T.-R. Chang, Z. Ye, G. Xu, M. M. Denner, T. Neupert, B. Lienhard, H.-B. Deng, C. Setty, Q. Si, G. Chang, Z. Guguchia, B. Gao, N. Shumiya, Q. Zhang, T. A. Cochran *et al.*, Discovery of charge order and corresponding edge state in kagome magnet FeGe, Phys. Rev. Lett. **129**, 166401 (2022).

[14] X. Teng, J. S. Oh, H. Tan, L. Chen, J. Huang, B. Gao, J.-X. Yin, J.-H. Chu, M. Hashimoto, D. Lu, C. Jozwiak, A. Bostwick, E. Rotenberg, G. E. Granroth, B. Yan, R. J. Birgeneau, P. Dai, and M. Yi, Magnetism and charge density wave order in kagome FeGe, Nat. Phys. **609**, 490 (2022).

[15] E. C. Stoner, Collective electron ferromagnetism, Proc. R. Soc. London A **165**, 372 (1938).

[16] Y. Xie, L. Chen, T. Chen, Q. Wang, Q. Yin, J. R. Stewart, M. B. Stone, L. L. Daemen, E. Feng, H. Cao, H. Lei, Z. Yin, A. H. MacDonald, and P. Dai, Spin excitations in metallic kagome lattice FeSn and CoSn, Commun. Phys. **4**, 240 (2021).

[17] Y.-X. Jiang, J.-X. Yin, M. M. Denner, N. Shumiya, B. R. Ortiz, G. Xu, Z. Guguchia, J. He, M. S. Hossain, X. Liu, J. Ruff, L. Kautzsch, S. S. Zhang, G. Chang, I. Belopolski, Q. Zhang, T. A. Cochran, D. Multer, M. Litskevich, Z.-J. Cheng *et al.*, Unconventional chiral charge order in kagome superconductor KV_3Sb_5, Nat. Mater. **20**, 1353 (2021).

[18] H. Zhao, H. Li, B. R. Ortiz, S. M. L. Teicher, T. Park, M. Ye, Z. Wang, L. Balents, S. D. Wilson, and I. Zeljkovic, Cascade of correlated electron states in a kagome superconductor CsV_3Sb_5, Nature (London) **599**, 216 (2021).

[19] A. Mielke and H. Tasaki, Ferromagnetism in the Hubbard model, Commun. Math. Phys. **158**, 341 (1993).

[20] T. Hanisch, B. Kleine, A. Ritzl, and E. Müller-Hartmann, Ferromagnetism in the Hubbard model: instability of the nagaoka state on the triangular, honeycomb and kagome lattices, Ann. Phys. **507**, 303 (1995).

[21] F. Pollmann, P. Fulde, and K. Shtengel, Kinetic ferromagnetism on a kagome lattice, Phys. Rev. Lett. **100**, 136404 (2008).

[22] Y. Ren, H.-C. Jiang, Z. Qiao, and D. N. Sheng, Orbital chern insulator and quantum phase diagram of a kagome electron system with half-filled flat bands, Phys. Rev. Lett. **126**, 117602 (2021).

[23] S. Nishimoto, M. Nakamura, A. O'Brien, and P. Fulde, Metal-insulator transition of fermions on a kagome lattice at 1/3 filling, Phys. Rev. Lett. **104**, 196401 (2010).

[24] A. O'Brien, F. Pollmann, and P. Fulde, Strongly correlated fermions on a kagome lattice, Phys. Rev. B **81**, 235115 (2010).

[25] J. Wen, A. Rüegg, C.-C. Joseph Wang, and G. A. Fiete, Interaction-driven topological insulators on the kagome and the decorated honeycomb lattices, Phys. Rev. B **82**, 075125 (2010).

[26] W. Zhu, S.-S. Gong, T.-S. Zeng, L. Fu, and D. N. Sheng, Interaction-driven spontaneous quantum Hall effect on a kagome lattice, Phys. Rev. Lett. **117**, 096402 (2016).

[27] Y. Ren, T.-S. Zeng, W. Zhu, and D. N. Sheng, Quantum anomalous Hall phase stabilized via realistic interactions on a kagome lattice, Phys. Rev. B **98**, 205146 (2018).

[28] Q. Liu, H. Yao, and T. Ma, Spontaneous symmetry breaking in a two-dimensional kagome lattice, Phys. Rev. B **82**, 045102 (2010).

[29] F. Pollmann, K. Roychowdhury, C. Hotta, and K. Penc, Interplay of charge and spin fluctuations of strongly interacting electrons on the kagome lattice, Phys. Rev. B **90**, 035118 (2014).

[30] S. Okamoto, N. Mohanta, E. Dagotto, and D. N. Sheng, Topological flat bands in a kagome lattice multiorbital system, Commun. Phys. **5**, 198 (2022).

[31] C. Setty, C. A. Lane, L. Chen, H. Hu, J.-X. Zhu, and Q. Si, Electron correlations and charge density wave in the topological kagome metal FeGe, arXiv:2203.01930 [cond-mat.str-el].

[32] D. P. Arovas, E. Berg, S. A. Kivelson, and S. Raghu, The Hubbard model, Annu. Rev. Condens. Matter Phys. **13**, 239 (2022).

[33] M. Qin, T. Schäfer, S. Andergassen, P. Corboz, and E. Gull, The Hubbard model: A computational perspective, Annu. Rev. Condens. Matter Phys. **13**, 275 (2022).

[34] See Supplemental Material at http://link.aps.org/supplemental/10.1103/PhysRevB.110.L041121 for details of the Hartree-Fock analysis, miscellaneous ground states in the pure Hubbard model, the effect of extended repulsion, mean-field renormalized band structure and band topology, and mean-field analysis of magnetic orders with PSG, which includes Refs. [73–79].

[35] D. A. Huse and V. Elser, Simple variational wave functions for two-dimensional heisenberg spin-$\frac{1}{2}$ antiferromagnets, Phys. Rev. Lett. **60**, 2531 (1988).

[36] J.-C. Domenge, P. Sindzingre, C. Lhuillier, and L. Pierre, Twelve sublattice ordered phase in the $J_1 - J_2$ model on the kagomé lattice, Phys. Rev. B **72**, 024433 (2005).

[37] J.-C. Domenge, C. Lhuillier, L. Messio, L. Pierre, and P. Viot, Chirality and $\mathbb{z}_2$ vortices in a heisenberg spin model on the kagome lattice, Phys. Rev. B **77**, 172413 (2008).

[38] L. Messio, C. Lhuillier, and G. Misguich, Lattice symmetries and regular magnetic orders in classical frustrated antiferromagnets, Phys. Rev. B **83**, 184401 (2011).

[39] K. Ohgushi, S. Murakami, and N. Nagaosa, Spin anisotropy and quantum Hall effect in the kagomé lattice: Chiral spin state based on a ferromagnet, Phys. Rev. B **62**, R6065 (2000).

[40] Y. Taguchi, Y. Oohara, H. Yoshizawa, N. Nagaosa, and Y. Tokura, Spin chirality, berry phase, and anomalous Hall effect in a frustrated ferromagnet, Science **291**, 2573 (2001).

[41] I. Martin and C. D. Batista, Itinerant electron-driven chiral magnetic ordering and spontaneous quantum Hall effect in triangular lattice models, Phys. Rev. Lett. **101**, 156402 (2008).

[42] K. Barros, J. W. F. Venderbos, G.-W. Chern, and C. D. Batista, Exotic magnetic orderings in the kagome kondo-lattice model, Phys. Rev. B **90**, 245119 (2014).

[43] V. J. Emery, S. A. Kivelson, and H. Q. Lin, Phase separation in the t-j model, Phys. Rev. Lett. **64**, 475 (1990).

[44] M. Qin, Effect of hole doping on the 120 degree order in the triangular lattice Hubbard model: a hartree-fock revisit, J. Phys.: Condens. Matter **34**, 235603 (2022).

[45] Here we are assuming that the (symmetry-breaking) commensurate orders are weak enough, and that the (possibly folded) bands develop a charge gap due to strong interactions.

[46] L. Balents, M. P. A. Fisher, and S. M. Girvin, Fractionalization in an easy-axis kagome antiferromagnet, Phys. Rev. B **65**, 224412 (2002).

[47] S. Yan, D. A. Huse, and S. R. White, Spin-liquid ground state of the $s = 1/2$ kagome heisenberg antiferromagnet, Science **332**, 1173 (2011).

[48] S. Nishimoto, N. Shibata, and C. Hotta, Controlling frustrated liquids and solids with an applied field in a kagome heisenberg antiferromagnet, Nat. Commun. **4**, 2287 (2013).

[49] H.-C. Jiang, Z. Wang, and L. Balents, Identifying topological order by entanglement entropy, Nat. Phys. **8**, 902 (2012).

[50] L. Messio, B. Bernu, and C. Lhuillier, Kagome antiferromagnet: A chiral topological spin liquid?, Phys. Rev. Lett. **108**, 207204 (2012).

[51] F. Wang and A. Vishwanath, Spin-liquid states on the triangular and kagomé lattices: A projective-symmetry-group analysis of schwinger boson states, Phys. Rev. B **74**, 174423 (2006).

[52] We note that a phase diagram for the self-consistent mean-field *Ansätze* obtained from PSG has been obtained in several works [50,79], where the SS order is absent. Here we follow a different interpretation for the *Ansätze*, and the SS order appears as a leading instability towards magnetic order—see [34] for a detailed discussion.

[53] H. Tan, Y. Liu, Z. Wang, and B. Yan, Charge density waves and electronic properties of superconducting kagome metals, Phys. Rev. Lett. **127**, 046401 (2021).

[54] Y.-P. Lin and R. M. Nandkishore, Complex charge density waves at van hove singularity on hexagonal lattices: Haldane-model phase diagram and potential realization in the kagome metals aV_3sb_5 (a=k, rb, cs), Phys. Rev. B **104**, 045122 (2021).

[55] T. Park, M. Ye, and L. Balents, Electronic instabilities of kagome metals: Saddle points and landau theory, Phys. Rev. B **104**, 035142 (2021).

[56] X. Feng, Y. Zhang, K. Jiang, and J. Hu, Low-energy effective theory and symmetry classification of flux phases on the kagome lattice, Phys. Rev. B **104**, 165136 (2021).

[57] M. H. Christensen, T. Birol, B. M. Andersen, and R. M. Fernandes, Theory of the charge density wave in av_3sb_5 kagome metals, Phys. Rev. B **104**, 214513 (2021).

[58] Y. Jiang, Z. Yu, Y. Wang, T. Lu, S. Meng, K. Jiang, and M. Liu, Screening Promising CsV_3Sb_5-Like kagome materials from systematic first-principles evaluation, Chin. Phys. Lett. **39**, 047402 (2022).

[59] G.-B. Jo, J. Guzman, C. K. Thomas, P. Hosur, A. Vishwanath, and D. M. Stamper-Kurn, Ultracold atoms in a tunable optical kagome lattice, Phys. Rev. Lett. **108**, 045305 (2012).

[60] A. Mazurenko, C. S. Chiu, G. Ji, M. F. Parsons, M. Kanász-Nagy, R. Schmidt, F. Grusdt, E. Demler, D. Greif, and M. Greiner, A cold-atom Fermi-Hubbard antiferromagnet, Nature (London) **545**, 462 (2017).

[61] H. Watanabe and M. Ogata, Charge order and superconductivity in two-dimensional triangular lattice at n=2/3, J. Phys. Soc. Jpn. **74**, 2901 (2005).

[62] X.-Y. Song, A. Vishwanath, and Y.-H. Zhang, Doping the chiral spin liquid: Topological superconductor or chiral metal, Phys. Rev. B **103**, 165138 (2021).

[63] C. Peng, Y.-F. Jiang, Y. Wang, and H.-C. Jiang, Gapless spin liquid and pair density wave of the Hubbard model on three-leg triangular cylinders, New J. Phys. **23**, 123004 (2021).

[64] Z. Zhu, D. N. Sheng, and A. Vishwanath, Doped mott insulators in the triangular-lattice Hubbard model, Phys. Rev. B **105**, 205110 (2022).

[65] Y. Huang, S.-S. Gong, and D. N. Sheng, Quantum phase diagram and spontaneously emergent topological chiral superconductivity in doped triangular-lattice mott insulators, Phys. Rev. Lett. **130**, 136003 (2023).

[66] Z. Zhu and Q. Chen, Superconductivity in doped triangular mott insulators: The roles of parent spin backgrounds and charge kinetic energy, Phys. Rev. B **107**, L220502 (2023).

[67] M. Cheng, K. Sun, V. Galitski, and S. Das Sarma, Stable topological superconductivity in a family of two-dimensional fermion models, Phys. Rev. B **81**, 024504 (2010).

[68] N. Gneist, D. Kiese, R. Henkel, R. Thomale, L. Classen, and M. M. Scherer, Functional renormalization of spinless triangular-lattice fermions: N-patch vs. truncated-unity scheme, Eur. Phys. J. B **95**, 157 (2022).

[69] Y. He, K. Yang, J. B. Profe, E. J. Bergholtz, and D. M. Kennes, Superconductivity of repulsive spinless fermions with sublattice potentials, Phys. Rev. Res. **5**, L012009 (2023).

[70] L. Savary and L. Balents, Quantum spin liquids: A review, Rep. Prog. Phys. **80**, 016502 (2017).

[71] Z. Liu and E. J. Bergholtz, Recent developments in fractional chern insulators, in *Reference Module in Materials Science and Materials Engineering* (Elsevier, Amsterdam, 2023).

[72] Y. Liu, Z.-Y. Liu, J.-K. Bao, P.-T. Yang, L.-W. Ji, J.-Y. Liu, C.-C. Xu, W.-Z. Yang, W.-L. Chai, J.-Y. Lu, C.-C. Liu, B.-S. Wang, H. Jiang, Q. Tao, Z. Ren, X.-F. Xu, C. Cao, Z.-A. Xu, J.-G. Cheng, and G.-H. Cao, Superconductivity emerged from

density-wave order in a kagome bad metal, arXiv:2309.13514 [cond-mat.supr-con].

[73] K. N. Kudin, G. E. Scuseria, and E. Cancès, A black-box self-consistent field convergence algorithm: One step closer, J. Chem. Phys. **116**, 8255 (2002).

[74] T. Fukui, Y. Hatsugai, and H. Suzuki, Chern numbers in discretized Brillouin zone: Efficient method of computing (spin) Hall conductances, J. Phys. Soc. Jpn. **74**, 1674 (2005).

[75] K. Sun, H. Yao, E. Fradkin, and S. A. Kivelson, Topological insulators and nematic phases from spontaneous symmetry breaking in 2d fermi systems with a quadratic band crossing, Phys. Rev. Lett. **103**, 046811 (2009).

[76] A. Szasz and J. Motruk, Phase diagram of the anisotropic triangular lattice Hubbard model, Phys. Rev. B **103**, 235132 (2021).

[77] T. Cookmeyer, J. Motruk, and J. E. Moore, Four-spin terms and the origin of the chiral spin liquid in mott insulators on the triangular lattice, Phys. Rev. Lett. **127**, 087201 (2021).

[78] D. Di Sante, B. Kim, W. Hanke, T. Wehling, C. Franchini, R. Thomale, and G. Sangiovanni, Electronic correlations and universal long-range scaling in kagome metals, Phys. Rev. Res. **5**, L012008 (2023).

[79] D. Rossi, J. Motruk, L. Rademaker, and D. A. Abanin, Schwinger boson study of the J_1-J_2-J_3 kagome Heisenberg antiferromagnet with Dzyaloshinskii-Moriya interactions, Phys. Rev. B **108**, 144406 (2023).